Spray Formation and Propagation in Open and Enclosed Reactors

U. Fritsching*[1,2], L. Buss[1], H.F. Meier[3], D. Noriler[4]
[1] Leibniz Institute for Materials Engineering – IWT Bremen, Bremen, Germany
[2] Department of Particle and Process Engineering, University of Bremen, Bremen, Germany
[3] Department of Chemical Engineering, University of Blumenau, Blumenau, Brazil
[4] School of Chemical Engineering, University of Campinas, Campinas, Brazil
*Corresponding author: ufri@iwt.uni-bremen.de

Introduction

Spray processes for particle and powder production typically are performed within an enclosed environment (spray tower or spray chamber). To synthesize metal and metal-oxide particles in nanoscale range, the flame spray pyrolysis (FSP) process can be applied and, in order to design advanced nanomaterials and to improve their properties, as well as to increase the production rate of the process, variations of such process and reactor/atomizer design have been analysed in several studies [1–5]. Most previous investigations on FSP process [6-9] consider an open reactor configuration which leads to a specific gas entrainment that primarily is controlled by the jet strength. However, with this setup, the control of the combustion environment is not so easy [10] and, depending on the requested particle characteristics, it might be hard to achieve them. Enclosing the reactor and applying a oxidizer co-flow gas allows to control the fuel-to-oxidizer ratio [11] in situations where it is required, such as for the synthesis of carbon black [12] and/or production of pure metal-oxide nanoparticles [13–15]. By enclosing the reactor, however, higher flame temperatures (since natural entrainment, and, therefore, its quenching effect is suppressed) and larger nanoparticles (since the particle coagulation and sintering are temperature-dependent) are observed [16]. In the conventional FSP process, a liquid precursor is dissolved in an organic fuel which is atomized into a spray of fine droplets. These droplets evaporate, and the vapor is instantaneously ignited due to the energy provided by a support flame. The fuel combustion produces enough energy to decompose and oxidize the precursor, resulting in a supersaturated environment of metallic oxide vapor which induces the particle nucleation and growth [17]. The spray formation and its propagation are affected by the shape and size of the enclosure as well as the amount of co-flowing gas, and, therefore, these phenomena in the enclosing spray chamber are to be controlled by flow control measures as, for instance, the superficial secondary gas flow.

In this contribution, spray processes for powder production – e.g. FSP process for nano-sized particle synthesis – is analyzed numerically by computational fluid dynamics (CFD) simulations. The role of the entrainment flow and recirculation areas in the enclosure is highlighted. In this sense, the influence of geometrical setups (open and enclosed reactor) at different operating conditions on the flame temperature and spray behavior as well as on the reactor temperature and temperature-residence-time distribution of the gas and the particles are investigated. Based on the natural gas entrainment into the spray flame, the appropriate amount of co-flowing gas satisfying the entrainment requirement of the spray is derived. Supplying this amount of co-flowing gas to the enclosed reactor setup results in a quite similar flame behavior as found for the open reactor. On the other hand, reducing the co-flow gas rate, strong vortex and recirculation zones are formed, which are typically observed in confined jets with reduced co-flow [18], and the temperature increases considerably, resulting in larger nanoparticle sizes [19]. The numerical results are analyzed and compared to the findings of previous studies.

Reactor Geometry and Numerical Domain

Figure 1 depicts a sketch of the two reactor setups used in this work. Figure 1a presents the open configuration, which consists of a twin-fluid atomizer surrounded by a support flame that is positioned in the center of a metallic plate. In the enclosed configuration, Figure 1b, the metallic plate is smaller and is surrounded by a porous plate, through the which the co-flowing gas is fed, positioned on the bottom of enclosure tube. The enclosure consists of a quartz tube with inner diameter of 0.1 m, height of 0.5 m and thickness of 0.003 m. The atomizer nozzle used here is described in detail by Mädler et al. [6]. The computational simulations are performed using a bi-dimensional (2D) axisymmetric approach, Figure 1c, in a numerical grid of ~175,000 hexahedral cells, considering a cylindrical domain with 0.1 m of diameter and 0.5 m of height. The applied computational mesh is refined in the region closest to the atomizer nozzle, where large gradients of velocity, temperature, and chemical species are found.

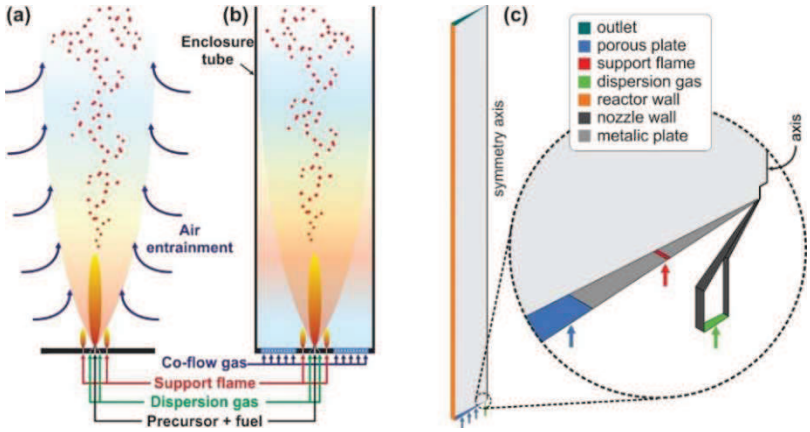

Figure 1. Sketch of FSP reactor in (a) open setup and (b) enclosed configuration; (c) 2D axisymmetric numerical domain.

Operating and Boundary Conditions

In this study, the boundary conditions (Table 1) are adjusted as adiabatic and impermeable wall for the nozzle and metallic plate walls; fixed mass flow for oxidant, support flame inlet and co-flow gas; and pressure boundary (fixed static pressure and zero gradients for the remaining variables) for the top and side limits (open reactor). Regarding the simulation setup applied to the enclosed configuration, heat transfer through the reactor walls must be considered since overestimation in the temperature distribution is expected when the reactor walls are adjusted to adiabatic condition, as has been demonstrated in the previous investigation [20]. The liquid phase consists of a precursor solution of zirconium *n*-propoxide (70 wt-% in *n*-propanol) and ethanol, with a total zirconium concentration of 0.5 mol/L. This solution is feed with a constant flow rate of 5 mL/min to the reactor and is atomized by 5 L/min dispersion oxygen, which gives a gas-to-liquid mass ratio (GLMR) of 1.7. The nozzle gap is adjusted to maintain a pressure drop of 1.5 x 10^5 Pa. The reactor operates either in open or enclosed condition, both at atmospheric pressure. In the enclosed configuration, air is supplied as co-flowing gas. From the open setup, the entrainment mass flow rate of gas is estimated. Several simulations (varying the gas co-flow rate) with the enclosed configuration are performed. These co-flow rates are 400 L/min (derived from estimations of entrainment gas with the open setup), 100 and 40 L/min. The liquid phase is already injected in the domain as spray droplets. The initial spray droplet size distribution is correlated by means of a Rosin-Rammler-Sperling-Bennet (RRSB) function to obtain the relevant parameters for the model setup and a stochastic Discrete Random Walk (DRW) model is applied to predict the turbulent droplet dispersion [21]. Proper droplet size distributions are obtained from previous studies [11, 22, 23].

Table 1. Boundary conditions assumed for numerical simulations.

Boundary name	Type	Value	Chemical composition
Dispersion gas	Mass-flow-inlet	1.19 x 10^{-4} kg/s (5 L/min)	100 wt-% O_2
Metallic plate	Wall	No-slip / Adiabatic	–
Nozzle wall	Wall	No-slip / Adiabatic	–
Outlet	Pressure-outlet	0 Pa	77 wt-% N_2 + 23 wt-% O_2
Support flame	Mass-flow-inlet	9.41 x 10^{-5} kg/s (4.7 L/min)	19 wt-% CH_4 + 81 wt-% O_2
Porous plate [a]	Wall	No-slip / Adiabatic	–
		8.50 x 10^{-3} kg/s (400 L/min)	
Porous plate [b]	Mass-flow-inlet	2.13 x 10^{-3} kg/s (100 L/min)	77 wt-% N_2 + 23 wt-% O_2
		8.50 x 10^{-4} kg/s (40 L/min)	
Reactor wall [a]	Pressure outlet	0 Pa	77 wt-% N_2 + 23 wt-% O_2
Reactor wall [b]	Wall	No-slip / Adiabatic	–

[a] For open reactor setup.

[b] For enclosed reactor setup.

Results and Discussion

Figure 2 presents CFD results concerning the gas velocity fields (a, c-e), gas entrainment (b) and gas recirculation (f) in a spray reactor. The mass flow of gas entrainment from the ambient – which is dragged into the spray region – increases with increasing the axial distance from the atomizer. Ricou and Spalding [24] proposed a linear correlation for the total mass flow rate of gas entrainment, $\dot{m}$, for a diffusion gas flame. Analysing the open setup (Figure 2a), the entrainment ratio at several heights above the burner, HAB, can be estimated (Figure 2b). By supplying sufficient amount of co-flow gas that satisfies the entrainment requirement of the spray – in this case ~400 L/min (Figure 2c) – a similar spray flow behavior and morphology as found in the open setup and negligible

recirculation are observed. In contrast, decreasing the co-flow rate (Figure 2d-e) strong vortex and recirculation zones are formed, which is typically observed in confined jets with reduced co-flow [18].

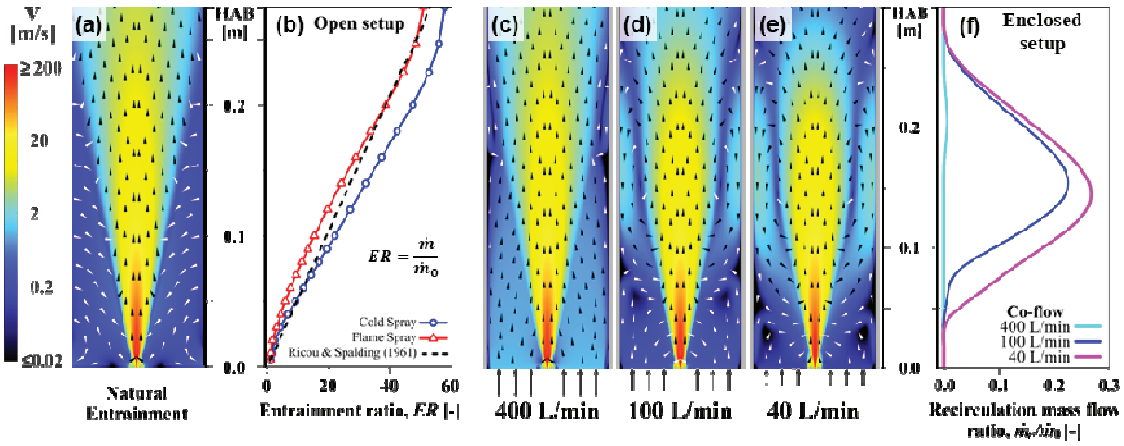

Figure 2. Gas velocity fields of open (a) and enclosed FSP reactor (c-e); analysis of entrainment ratio (b) at several heights above the burner (HAB) in an open FSP reactor and recirculation mass flow ratio (f) in an enclosed FSP reactor.

Figure 3 shows the predicted temperature distributions, the particle-residence-time, PRT as function of temperature, and primary particle diameter as function of HAB for the different investigated cases. In the open reactor and enclosed setup with 400 L/min co-flowing gas (Figure 3a and b, respectively), the temperature fields are quite similar, confirming the appropriate co-flowing gas is supplied. Reducing the co-flow also increases the reactor temperature fields, since the amount of quenching gas supplied to the reactor is lower and the recirculation of hot gas is stronger. As is shown in Figure 3b-d, the lower co-flow rates are, the stronger the vortex formation and recirculation zones become, leading, in turn, to higher temperature in the downstream of the reactor. The gas recirculation also increases the PRT in the flame/hot regions (Figure 3e) which results in larger particle formation (Figure 3f) with lower co-flowing gas rates. For the open configuration, the PRT has a maximum of ~0.10 s at just 450 K while for the enclosed setup with the lower co-flow rate, the maximal PRT is ~0.35 s (at 600 K). For temperature > 600 K, the PRT of the open and enclosed reactor with 400 L/min co-flowing gas present quite similar results, again, corroborating the appropriate co-flow gas is provided. As nanoparticle coagulation and sintering are determined by the temperature history, particles with similar size distribution are produced by both open and enclosed with 400 L/min configurations, since similar PRT in the same temperature range are found. Decreasing the gas co-flow rate extends the PRT in the high temperature zones. For the case with 40 L/min co-flowing gas, at 1500 K, the PRT is ~0.16 s and reaches values smaller than 0.005 s in the regions with temperatures of ~2250 K only. As observed in Figure 3f, the PRT in the high temperature zones impacts directly the powder size distribution. The longer the PRT in high-temperature regions, the larger is the size of produced particles.

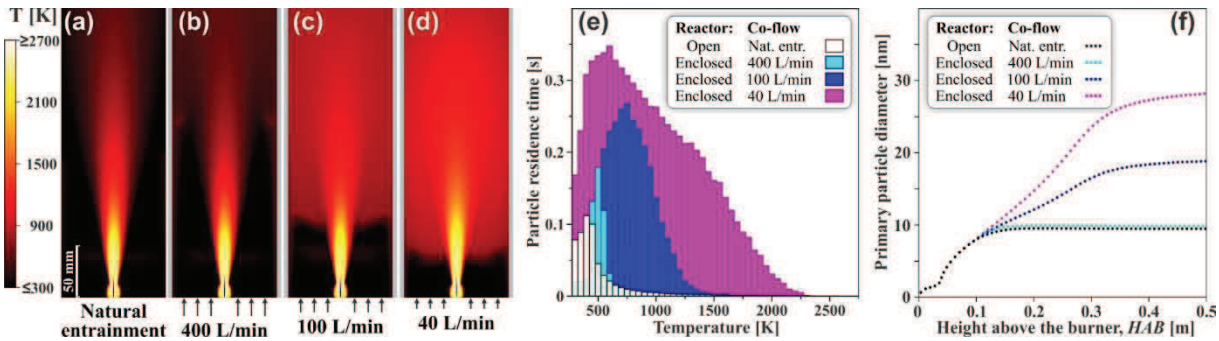

Figure 3. Simulated temperature fields of open (a) and enclosed FSP reactor (b-c); particle-residence-time, TRT, (e) and primary particle diameter (f) for the open and enclosed setups and different co-flow rates.

Nomenclature

$\dot{m}_0$	initial mass flow rate [kg s^{-1}]
$\dot{m}_r$	recirculation mass flow rate [kg s^{-1}]
$\dot{m}$	mass flow rate [kg s^{-1}]
CFD	computational fluid dynamics
DRW	Discrete Random Walk model
ER	entrainment ratio

FSP flame spray pyrolysis
GLMR gas-to-liquid mass ratio
HAB height above the burner [m]
PRT particle-residence-time [s]
RRSB Rosin-Rammler-Sperling-Bennet function

Acknowledgments
This contribution has received funding from the German Research Foundation – DFG (Project ID: FR912/33) and Coordination for the Improvement of Higher Education Personnel – CAPES (Process ID: BEX 12369/12-8) and is part of the framework program of the Brazilian-German Collaborative Research Initiative on Manufacturing Technology – BRAGECRIM (Project ID: 20/2012). Additional acknowledgement is also directed to The São Paulo Research Foundation – FAPESP, in Brazil (Project ID: 2017/04045-0).
The results reported here have been presented at the DIPSI Workshop 2018 in Bergamo and parts were also presented at ICLASS 2018 in Chicago [11].

References
[1] Fritsching, U., Spray Systems, in Multiphase Flow Handbook, CRC Press, Boca Raton, 2006.
[2] Fritsching, U., Uhlenwinkel, V., “Hybrid Gas Atomization Powder Production,” in *Powder Metallurgy*, In Tech, 2012.
[3] Lagutkin, S., Achelis, L., Sheikhaliev, S., Uhlenwinkel, V., Srivastava, V., *Materials Science and Engineering A,* 383: 1-6 (2004).
[4] Meierhofer, F., Hodapp, M. J., Achelis, L., Buss, L., Noriler, D., Meier, H. F., Fritsching, U., *Materials Science and Engineering Technology,* 45: 765-778 (2014).
[5] Achelis, L., Meierhofer, F., Hodapp, M. J., Buss, L., Noriler, D., Meier, H. F., Fritsching, U., *Proceedings of the ASME 2014 - 4th Joint US-European Fluids Engineering Division Summer Meeting,* 3-7 August 2014.
[6] Mädler, L., Kammler, H. K., Mueller, R., Pratsinis, S. E., *Journal of Aerosol Science,* 33: 369-389 (2002).
[7] Mädler, L., *KONA Powder and Particle Journal*, 22: 107-120 (2004).
[8] Mädler, L., Roessler, A., Pratsinis, S. E., Sahm, T., Gurlo, A., Barsan, N., Weimar, U., *Sensors and Actuators,* 114: 283-295 (2006).
[9] Gröhn, A. J., Pratsinis, S. E., Wegner, K., *Chemical Engineering Journal,* 191: 491-502 (2012).
[10] Waser, O., Groehn, A. J., Eggersdorfer, M. L., Pratsinis, S. E., *Aerosol Science and Technology,* 48: 1195-1206 (2014).
[11] Buss, L., Bianchi Neto, P., Meier, H. F., Fritsching, U., Noriler, D., *ICLASS 2018 - 14th Triennial International Conference on Liquid Atomization and Spray Systems,* 22-26 July 2018.
[12] Waser, O., Büchel, R., Hintennach, A., Novák, P., Pratsinis, S. E., *Journal ofAerosol Science,* 42: 657-667 (2011).
[13] Athanassiou, E. K., Grass, R. N., Stark, W. J., *Nanotechnology,* 17: 1668-1673 (2006).
[14] Waser, O., Brenner, O., Groehn, A. J., Pratsinis, S. E., *Chemical and Process Engineering,* 38: 51-66 (2017).
[15] Buss, L., Meierhofer, F., Noriler, D., Meier, H. F., Fritsching, U., *ILASS - Europe 2016, 27th Annual Conference on Liquid Atomization and Spray Systems,* 4-7 September 2016.
[17] Teoh, W. Y., Amal, R., Mädler, L., *Nanoscale,* 2: 1324-1347 (2010).
[18] Curtet, R., *Combustion and Flame,* 2: 383-411 (1958).
[19] Waser, O., Hess, M., Güntner, A., Novák, P., Pratsinis, S. E., *Journal of Power Sources,* 241: 415-422 (2013).
[20] Meierhofer, F., Buss, L., Noriler, D., Meier, H. F., Fritsching, U., *ICMF 2016 - 9th International Conference on Multiphase Flow,* 22-27 May 2016.
[21] Gosman, A. D., Ioannides, E., *Journal of Energy,* 7: 482-490 (1983).
[22] Noriler, D., Rosebrock, C. D., Mädler, L., Meier, H. F., Fritsching, U. *Atomization and Sprays,* 24: 495-524 (2014).
[23] Bianchi Neto, P., Buss, L., Meierhofer, F., Meier, H. F., Fritsching, U., Noriler, D., *Chemical Engineering and Processing,* 129: 17-27 (2018).
[24] Ricou, F. P., Spalding, D. B., *Journal of Fluid Mechanics,* 11: 21-32 (1961).